Stability of Cylindrical and Conical Hypersonic Boundary Layers

Geoffrey M. Andrews* and Jonathan Poggie.†
Purdue University, West Lafayette, IN, USA, 49707

Hypersonic boundary layers are analyzed using linear stability theory, augmented by direct numerical simulation. Cylindrical and conical boundary layers, their receptivity to freestream disturbances, and subsequent paths to laminar-turbulent transition are investigated. Artificial disturbances are input to each boundary layer via a periodic blowing-suction technique which creates velocity fluctuations at a desired frequency; direct numerical simulation is used to analyze the downstream growth of these perturbations. Results from the linear stability theory analysis show good agreement with published experimental data, which is supported by the completed direct numerical simulations.

I. Introduction

HYPERSONIC boundary layer transition has developed a well-deserved reputation as one of the great unsolved mysteries of aerodynamics. Despite its critical importance to the development of a range of flight technologies, such as space access systems and high-speed air transport, the phenomena of laminar-turbulent transition is not well-understood. Perhaps the greatest challenge in the field is the prediction of transition location. Understanding where a flight vehicle's boundary layer should transition from laminar to turbulent is critically important as the turbulent hypersonic flows have been shown to significantly increase skin friction and heating rates, confounding the process of hypersonic vehicle design.

Although the hypersonic transition problem is one of key importance, a detailed understanding of the phenomenon remains beyond the state of the art. A variety of correlations (such as the common e^N method) have been proposed over the years, with varying degrees of accuracy. Most, if not all, of these correlations are semi-empirical, requiring at least some degree of tuning to match a given flight test or experimental facility.

Due to the intense sensitivity of hypersonic flows to minute irregularities in surface finish, heating/cooling, freestream impurities, ambient noise, and a host of other factors, experimental data for hypersonic boundary layer transition are infamously opaque. It can be almost impossible to ascertain whether observed data are truly indicative of relevant physical processes or artifacts of suboptimal facility or experimental setup. In particular, there is a consensus that facility noise has played a dominant role in many critical experiments conducted over the past several decades [1–5]. At hypersonic velocities, turbulent boundary layers which form on the walls of tunnel test sections radiate a significant amount of acoustic disturbance into the freestream; these disturbances are converted into boundary layer instabilities through receptivity processes. Pate performed early research into radiated noise phenomena [6]; a more modern review of the topic has been published by Schneider [7].

One method to ameliorate this confusion is through the development of quiet tunnels such as those currently operating at Purdue [8], Texas A& M [9], and China's NUDT [10]. Although these tunnels offer greater insight into turbulent transition phenomena, the scarcity of these facilities and the high cost of building new ones make alternative solutions quite appealing. Specifically, the growth of high-performance, massively parallel computing capabilities in recent years offers new hope for finding deeper insights into the hypersonic transition problem.

One enduring puzzle within the realm of hypersonic boundary layer transition is an observed difference in behaviour between conical and planar boundary layers. Classical laminar boundary layer theory suggests that conical and planar boundary layers should differ in their streamwise development by a factor of three (i.e. the boundary layer at a particular point on a plate should be identical to the boundary layer at a point three times farther downstream on a cone) - a result which can be derived from integration of the boundary layer form of the momentum equation around a solid of revolution [11]. An experimental analysis of transition-point Reynolds numbers for cones at Mach 3.0 by Potter and Whitfield [12] supported this idea, but later work by Pate [13] found a value for the transition Reynolds number ratio which ranged from 2.5-1.0 across a Mach number range of 3 to 8.

*Ph.D. Student, School of Aeronautics and Astronautics, AIAA Student Member.
†Associate Professor, School of Aeronautics and Astronautics, AIAA Associate Fellow.

Mack called this theory further into question by applying principles of linear stability theory [14]; he suggested that the transition Reynolds number should actually be *higher* for a flat plate than for a cone [15]. This position was further supported by experiments performed at NASA Langley in the Mach 3.5 quiet tunnel, which found the transition Reynolds number ratio to vary between 0.8-1.2 for the low-noise Mach 3.5 condition, in which first-mode disturbances might be expected to dominate. A further study by Stetson et al. [16] examined the problem of transition on sharp cones at Mach 8, a flow regime in which second-mode instabilities are more significant than first-mode instabilities. Interestingly, Stetson et al. found that in conical boundary layers, transition Reynolds numbers were indeed higher than they were in cylindrical boundary layers, contradicting the results of Mack's linear stability analysis. This study also suggested that the growth rates for second-mode instabilities are lower in planar boundary layers than in conical boundary layers. The authors' conclusion was that for planar boundary layers, low-frequency first-mode instabilities dominate transition, whereas in conical boundary layers, second-order disturbances are the dominant transition phenomenon. Later work by Zhong [17] suggested that the location of the synchronization point between the first and second modes could explain this counterintuitive behaviour, although Zhong's simulations were constrained to conical boundary layers, and did not address the flat-plate case. The available literature seems to indicate that there is a difference in the receptivity process between cylindrical and conical boundary layers; however, the specifics of the process for each case and the root cause for the observed differences remains unclear.

The goal of the present study is to further analyze the seemingly contradictory measurements present in the literature for conical and planar boundary layers at hypersonic freestream velocities. Specifically, this work aims to examine the hitherto unexplained differences in receptivity between cylindrical and conical boundary layers [16] and gain some insight into the differences in observed amplification rates of first- and second-mode instabilities in the two geometries.

The behaviour of cylindrical and conical boundary layers will be studied using a combination of linear stability theory (LST) and direct numerical simulation (DNS). The LST analysis will attempt to capture the unexpected second-mode damping and first-mode amplification observed by Stetson et al., for their cylindrical boundary layer. The DNS will attempt to reproduce this result computationally using forced disturbances in each boundary layer, as demonstrated by Zhong & Ma [18] and Egorov et al. [19]. This method works by imposing a periodic blowing/suction input near the leading edge of each geometry; this creates an instability with a controllable frequency which enables the study of particular instability modes in each boundary layer. While Egorov et al. were able to successfully demonstrate this technique in two dimensions, the present study will implement it in three dimensions and use it as a tool to compare the behaviour of the conical and cylindrical boundary layers.

II. Laminar Base Flow

For each boundary layer analysis, a solution for the undisturbed, steady-state laminar base flow was required. These calculations were performed using the Higher-Order Plasma Solver (HOPS) code. HOPS was created by Dr. Jonathan Poggie at the United States Air Force Research Laboratory [20]; although originally written to simulate non-equilibrium flows for the study of plasmas, it is also capable of accurately capturing fluid flows [21]. For this study, a sixth-order compact difference spatial discretization scheme is used (with a reduction to fourth-order at the domain boundaries and application of the Roe scheme near shocks). Freestream conditions come directly from the experiments of Stetson et al. and are presented in Table 1.

Table 1: Flow Conditions

Mach Number (M_∞)	7.94
Freestream velocity (u_∞)	1176.0 m/s
Static Pressure (P_∞)	165.5 Pa
Static Temperature (T_∞)	54.4 K
Density (ρ_∞)	1.059×10^{-2} kg/m^3
Unit Reynolds Number (Re_∞)	3.20×10^6 m^{-1}
Wall temperature (T_w)	305.7 K

These laminar base flow solutions were obtained by running calculations for the basic states of the cone and cylinder until convergence was reached. Grid refinement was carried out to ensure well-resolved solutions; the final grid

employed clustering in both the near-wall and the entropy-layer regions of the boundary layer. Contours of normalized pressure are shown for the two base flow solutions in Figure 1.

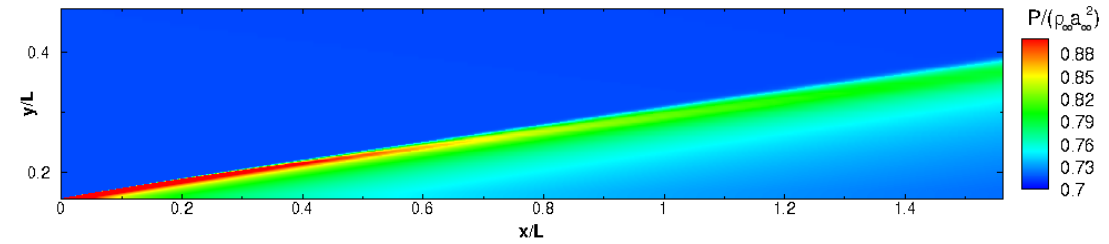

(a) Cylinder

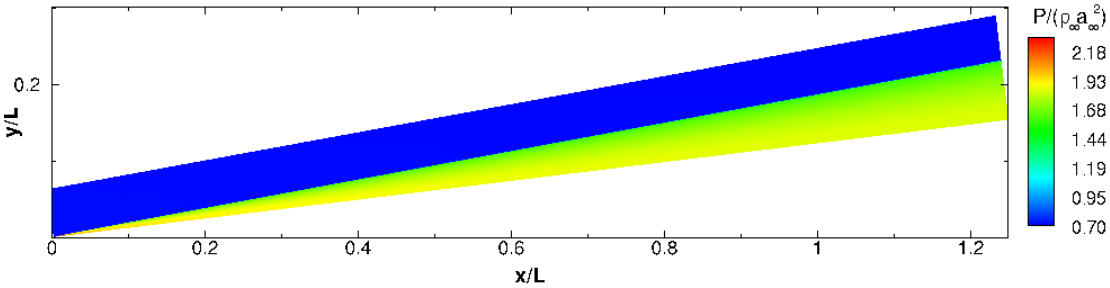

(b) Cone

Fig. 1: Pressure contours for laminar base flow solutions.

III. Linear Stability Theory

One established method for analyzing the stability of boundary layers is Linear Stability Theory (LST). LST relies upon a linearization of the Navier-Stokes equations, which are then solved for perturbation flow quantities. The Langley Stability and Transition Analysis Code (LASTRAC) was used to further investigate the stability of periodic boundary layer disturbances in two dimensions. Stability diagrams generated by LASTRAC are shown below. These diagrams provide an indication of the relative amplification of disturbances of different frequencies as they propagate through the boundary layer. The contours represent instability growth rates, where red denotes maximum amplification, blue denotes approximately neutral stability, and white damping.

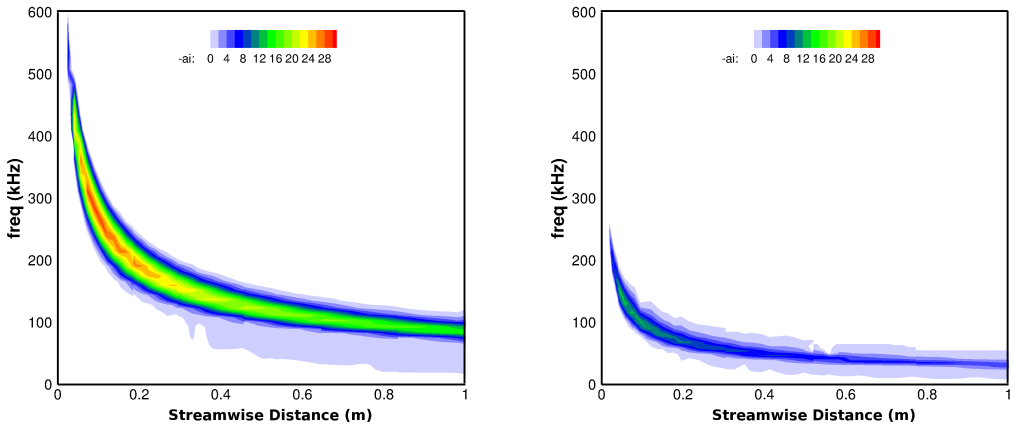

(a) Cone **(b) Cylinder**

Fig. 2: Stability diagrams for the geometries of Stetson et al.

This analysis reveals key differences between conical and cylindrical boundary layers. For the cone of Stetson et al., higher-frequency second-mode instabilities seem to dominate, whereas for the corresponding cylindrical boundary layer, lower-frequency instabilities are more amplified (though to a lesser extent than the cone). The present analysis does not capture any amplification of first-mode instabilities since these are a three-dimensional phenomenon.

LASTRAC was used to calculate the predicted growth of disturbances of various frequencies in each boundary layer. Following the e^N method, the integrated growth rates yield a value of N which describes the amplification of a given disturbance frequency as it propagates through the boundary layer. At some critical value of N, the linear disturbances break down to turbulence. N-factors calculated using LASTRAC are shown below in Figure 3.

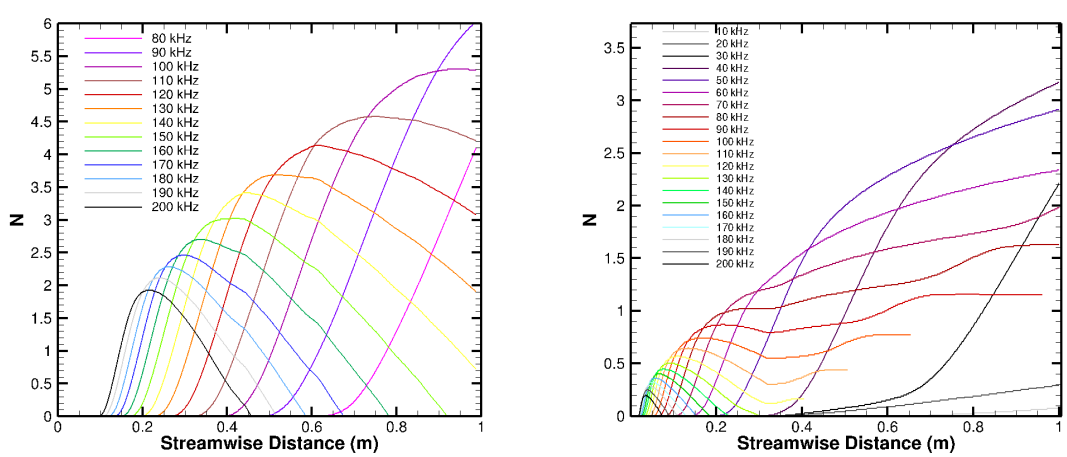

(a) Cone **(b) Cylinder**

Fig. 3: N-factors for each the geometries of Stetson et al.

The N-factor curves provide a clear indication of which disturbance frequencies are most unstable. They suggest that in the initial stages of the linear growth region, the higher-frequency disturbances near 200 kHz are more unstable; farther downstream,lower frequencies are amplified more. At the transition points reported by Stetson et al. (x = 0.686 m and x = 0.813 m for the cone and cylinder, respectively), the most unstable frequencies as indicated by the calculated N factors are approximately 90 kHz and 50 kHz, respectively. These frequencies correspond very closely with the

disturbance amplitude spectra shown by Stetson et. al (copied in Figure 4). These plots follow the example of Stetson et al., showing the overall amplitude of disturbances in arbitrary units plotted against the disturbance frequency in kHz. Each line represents different Reynolds number calculated from conditions at the boundary layer edge and the streamwise distance. Qualitative agreement between the plots is apparent: although the frequency bands differ slightly between the computed and measured results, the relative magnitudes of the disturbance amplitudes appears quite consistent. The wide low-frequency band which appears amplified in experimental measurements of both the cone and cylinder is likely a result of facility noise.

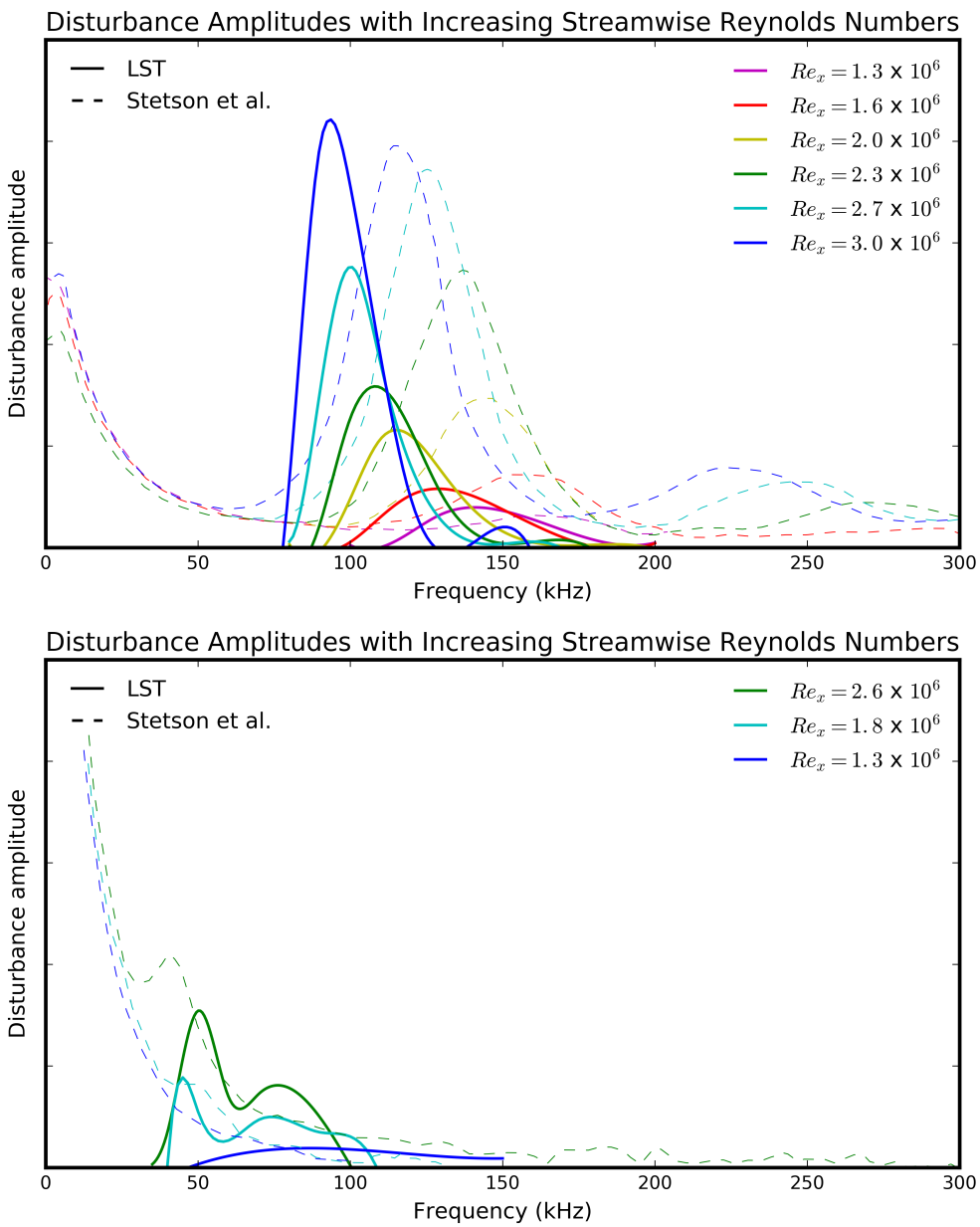

Fig. 4: Cylinder disturbance amplitudes with increasing streamwise Reynolds numbers; LST calculations and experimental data [16] shown for conical boundary layer (top) and cylindrical boundary layer (bottom).

In addition to the qualitative agreement in disturbance amplitudes, the maximum growth rates at each point in the two boundary layers (shown in Figure 5), align well with the data of Stetson et al. for the amplification of second-mode instabilities.

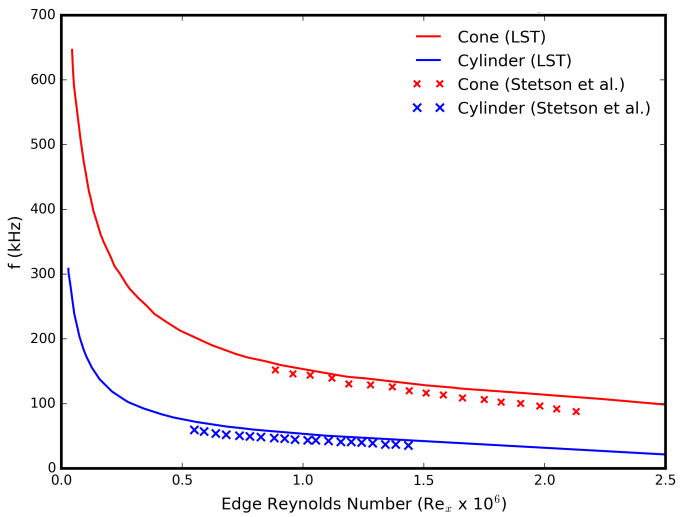

Fig. 5: Maximum growth rates of second-mode frequencies.

It is possible to analyze the modal structure of the boundary layer disturbances by using LASTRAC to extract the characteristic eigenfunctions associated with each frequency. The eigenfunctions for the conical boundary layer appear to fall into two approximate groupings. The first of these is the dominant second-mode disturbance between 70 and 110 kHz, which are the highest-amplitude disturbances. A second eigenmode distribution is also present between the frequencies of 120 and 200 kHz.

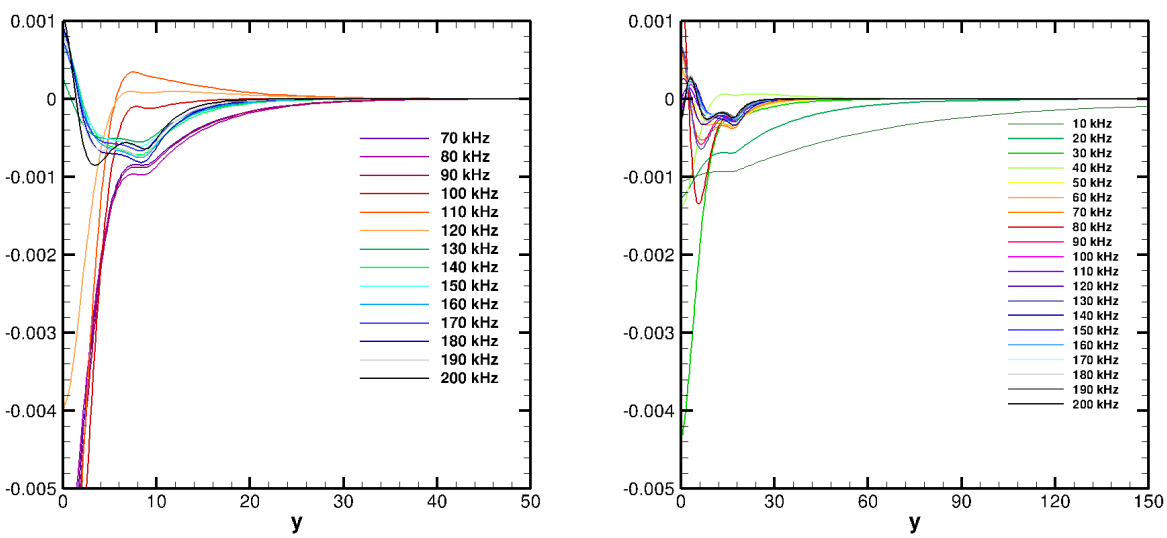

(a) Cone **(b) Cylinder**

Fig. 6: Eigenmodes of pressure plotted against wall-normal coordinates for the geometries of Stetson et al.

The eigenfunctions for the cylindrical boundary layer seem to be dominated by lower-frequency disturbances; as

mentioned above these are most likely the result of facility noise captured by the boundary layer. These are followed by the higher-frequency second-mode instability waves; the highest-frequency harmonics round out the eigenmode distribution. Overall, LST analysis shows good agreement with the stability behavior observed by Stetson et al. [16].

IV. Direct Numerical Simulation

The HOPS code was used to carry out direct numerical simulation for the conditions reported by Stetson et al. for their cone and hollow cylinder at a Reynolds number of $Re = 1.0 \times 10^6$ ft^{-1}. The freestream conditions are the same as those in Table 1 and the two computational domains encompassed the entire clean length of each test article: 1.270 m for the cylinder and 1.016 m for the cone. Distances shown are normalized by the experimentally-observed cylinder transition location, $x = 0.813m$. For the cylindrical case, the computational mesh contained 5.6×10^8 points, with high resolution in the azimuthal direction in order to permit the flow to break down and transition to turbulence. In the conical mesh, which contained 9.0×10^7 points, this was not possible due to the model geometry; the mesh was coarsened azimuthally to avoid extremely small cells created by the nose tip's smaller circumference. Each grid implemented clustering near the wall and stretching near the upper and outflow boundaries to create a sponge layer. The numerical scheme employed sixth-order compact differencing with eighth-order filtering for all continuous regions of the flow, with a second-order Roe scheme near shocks. Disturbances were input to the laminar base flow solutions using an artificial blowing-suction boundary condition applied to a patch of the flow surface. Specifically, the flow-normal velocity is given a sinusoidal profile at this point, described by the following expression (provided by Egorov et al.) [19],

$$v(x) = A \sin\left(2\pi \frac{x - x_1}{x_2 - x_1}\right) \sin(2\pi\omega t), \tag{1}$$

where A is the initial disturbance amplitude, x_1 and x_2 are the streamwise boundaries of the blowing-suction region, and ω is the disturbance frequency. This artificial input makes it possible to study the behavior of disturbances of different frequencies as they propagate downstream.

Cylindrical and conical cases were run to establish laminar base flows, and then forced with the maximally-unstable frequencies indicated by the LST analysis. For the cylinder, this was 50 kHz; for the cone, 90 kHz. Results obtained with this approach are shown below. Figure 7 shows the normalized difference in pressure between the perturbed flow and the base flow for the cylindrical case; Figure 8 shows the same quantity for the conical case.

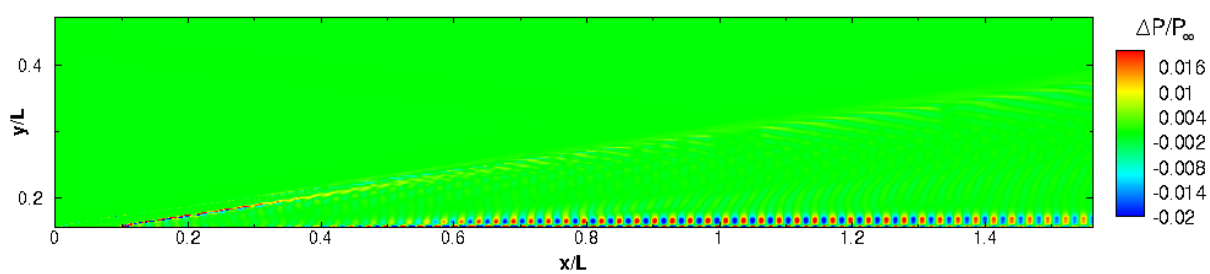

Fig. 7: Cylindrical boundary layer perturbed at 50 kHz.

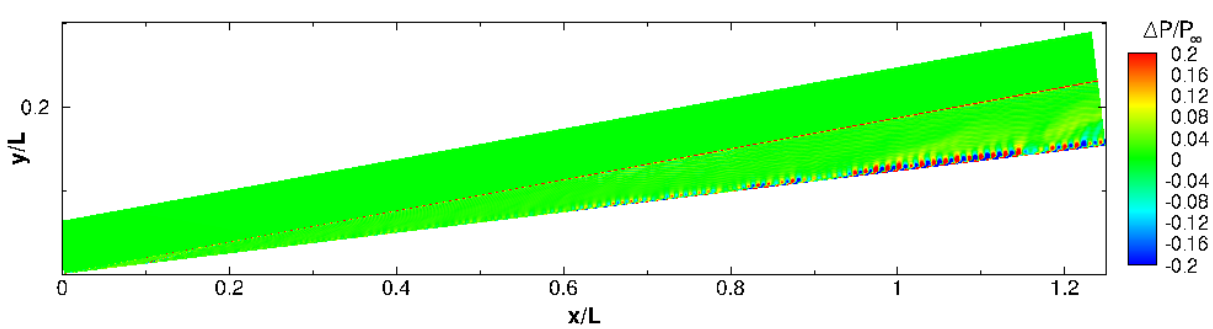

Fig. 8: Conical boundary layer perturbed at 90 kHz.

In both figures, the characteristic features of the flow disappear, leaving a weak shock generated at the disturbance input location ($x/L = 1$) and a gradually-growing disturbance in the boundary layer. Figures 9 and 10 show detailed comparisons of the base and perturbed flows near the exit of each computational domain. Contours of pressure (normalized by freestream conditions) are shown for each case.

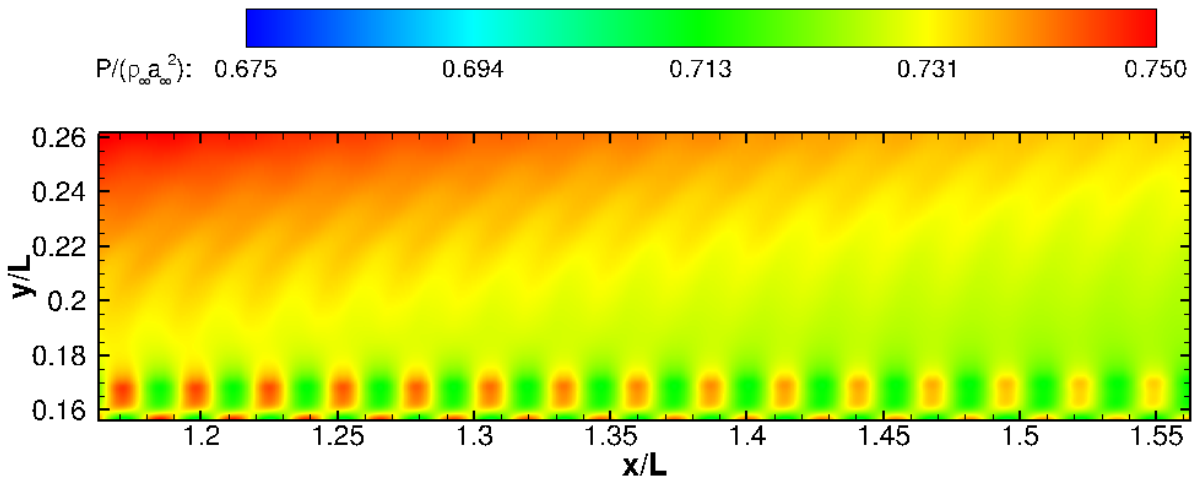

Fig. 9: DNS of cylindrical boundary layer with 50 kHz artificial disturbance.

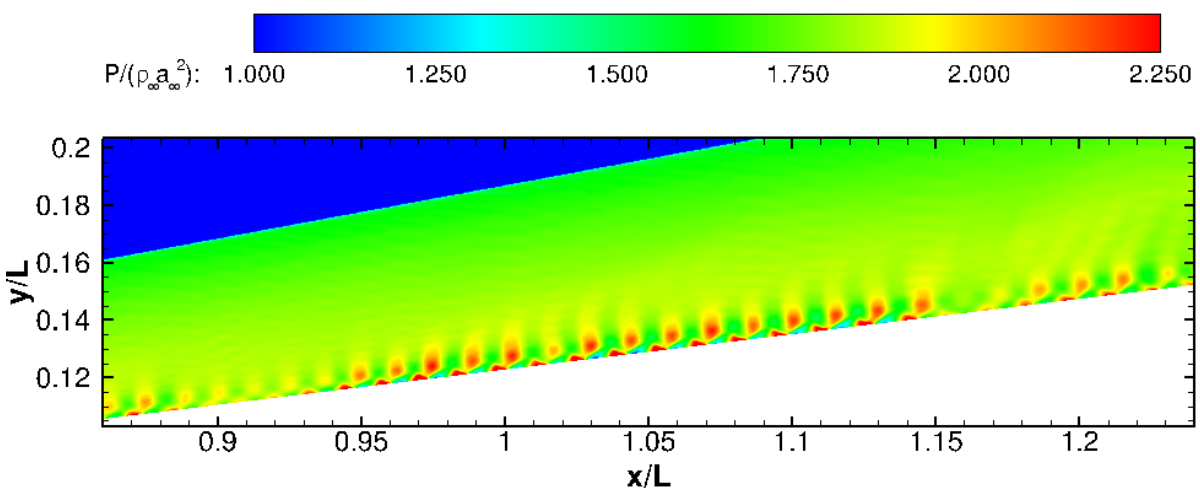

Fig. 10: DNS of conical boundary layer with 90 kHz artificial disturbance.

The perturbed flows show the clear periodic structures created by the upstream disturbances, as well as acoustic noise radiating upwards towards the shocks. The conical case seems to indicate nonlinear growth, possibly as a result of modal interaction (which is captured by HOPS but not the LASTRAC LST analysis). These images show that it is possible to simulate the growth of boundary layer disturbances by that are computationally input via a suction-blowing method within HOPS.

Comparison with the disturbance growth predicted by LASTRAC shows good agreement between DNS and LST calculation. The overall amplitude of the cylindrical boundary layer disturbance from the HOPS calculation roughly matches the disturbance amplitude calculated using LASTRAC, as shown in Figure 11.

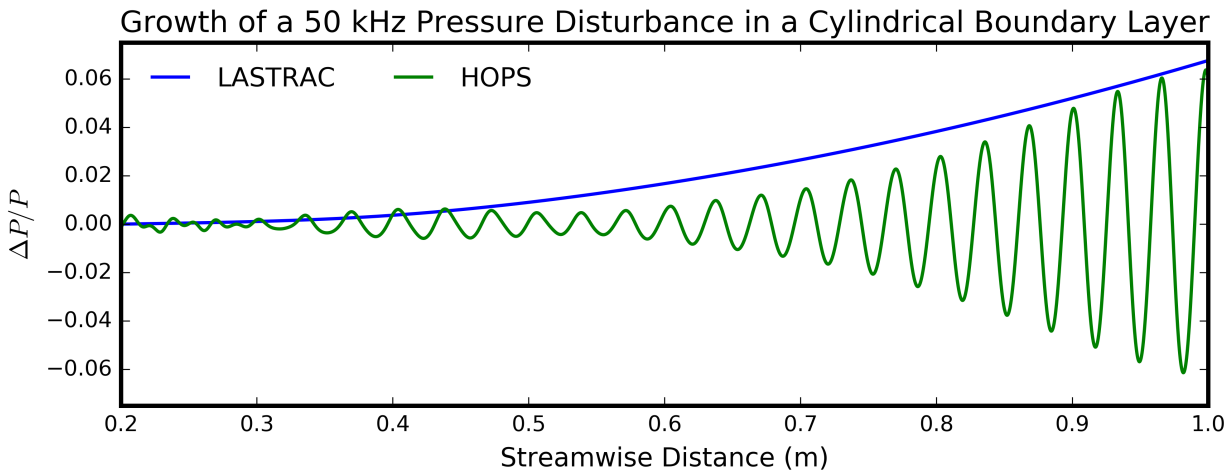

Fig. 11: Comparison between HOPS and LASTRAC calculations.

V. Conclusions

The linear stability theory analysis presented in this paper agrees with the experimental findings of Stetson et al. in that it shows markedly lower growth rates for second-mode instabilities in a high-speed cylindrical boundary layer when compared to an equivalent conical boundary layer. In addition, the cylinder amplifies lower-frequency disturbances which do not appear prominently in the conical boundary layer. In light of the LST results, examination of the disturbance amplitudes reported by Stetson et al. suggests that the low-frequency waves measured in both conical and cylindrical boundary layers are largely a result of facility noise.

To better understand the complex nonlinear interactions which appear to drive high-speed transition, direct numerical simulation using the Higher-Order Plasma Solver (HOPS) code with periodic blowing-suction disturbances has been introduced. Early results from HOPS corroborate the findings of the LST analysis and indicate that the code is a capable tool for analyzing the development of instabilities in high-speed boundary layers.

As a continuation of this work, the authors are currently performing further detailed analysis using HOPS by introducing a multitude of individual forcing frequencies. The eventual goal is to simulate the introduction of disturbances in the form of a simulated wavepacket traveling the freestream, so as to better understand the receptivity process which converts freestream disturbances into boundary layer instabilities.

VI. Acknowledgements

This work was supported by ONR Grant N000141712374, monitored by Dr. Eric Marineau, and computer time was provided through a DoD HPCMP Frontier Project. The authors would like to thank Dr. Chau-Lyan Chang and Dr. Matthew Tufts for their kind and generous assistance with the LASTRAC code, as well as the HPCMP technical support staff.

References

[1] Laufer, J., "Factors affecting transition Reynolds numbers on models in supersonic wind tunnels," *Journal of the Aeronautical Sciences*, Vol. 21, No. 7, 1954, pp. 497–498.

[2] Pate, S. R., and Scheuler, C., "Radiated aerodynamic noise effects on boundary-layer transition in supersonic and hypersonic wind tunnels," *AIAA Journal*, Vol. 7, No. 3, 1969, pp. 450–457.

[3] Stainback, P. C., "Hypersonic boundary-layer transition in the presence of wind-tunnel noise," *AIAA Journal*, Vol. 9, No. 12, 1971, pp. 2475–2476.

[4] Reshotko, E., "Boundary-layer stability and transition," *Annual Review of Fluid Mechanics*, Vol. 8, No. 1, 1976, pp. 311–349.

[5] Beckwith, I. E., and Miller, I., C. G., "Transition in High-Speed Wind Tunnels at NASA Langley," *Annual Review of Fluid Mechanics*, Vol. 22, No. 1, 1990, pp. 419–439.

[6] Pate, S. R., "Dominance of Radiated Aerodynamic Noise on Boundary-Layer Transition in Supersonic-Hypersonic Wind Tunnels - Theory and Application," AEDC-TR-77-107, 1978.

[7] Schneider, S. P., "Effects of High-Speed Tunnel Noise on Laminar-Turbulent Transition," *Journal of Spacecraft and Rockets*, Vol. 38, No. 3, 2001, pp. 323–333. doi:10.2514/2.3705.

[8] Schneider, S. P., "Design and Fabrication of a 9.5-inch Mach-6 Quiet-Flow Ludwieg Tube," AIAA Paper 98-2511, 1998. doi:10.2514/6.1998-2511.

[9] Hofferth, J., Bowersox, R., and Saric, W., "The Mach 6 Quiet Tunnel at Texas A&M: Quiet flow performance," AIAA Paper 2010-4794, 2010.

[10] Gang, D., Yi, S., and Lu, X., "Design and performance of a hypersonic quiet wind tunnel at NUDT," AIAA Paper 2017-2305, 2017. doi:10.2514/6.2017-2305.

[11] Hantzsche, W., and Wendt, H., "The Laminar Boundary Layer on a Cone in a Supersonic Air Stream at Zero Angle of Attack," DTIC Report AD0604783, 1947.

[12] Leith Potter, J., and D. Whitfield, J., "Effects of slight nose bluntness and roughness on boundary-layer transition in supersonic flows," *Journal of Fluid Mechanics*, Vol. 12, 1962, pp. 501 – 535.

[13] Pate, S. R., "Measurements and Correlations of Transition Reynolds," *AIAA Journal*, Vol. 9, No. 6, 1971, pp. 1082–1090. doi:doi:10.2514/6.1970-799.

[14] Mack, L., "Linear Stability Theory and the Problem of Supersonic Boundary- Layer Transition," *AIAA Journal*, Vol. 13, No. 3, 1975, pp. 278–289. doi:10.2514/3.49693.

[15] Mack, L., "Stability of axisymmetric boundary layers on sharp cones at hypersonic Mach numbers," AIAA Paper 1987-1413, 1987. doi:10.2514/6.1987-1413.

[16] Stetson, K., Kimmel, D., R., J., and Siler, L., "A comparison of planar and conical boundary layer stability and transition at a Mach number of 8," AIAA Paper 1991-1639, 1991. doi:10.2514/6.1991-1639.

[17] Zhong, X., "Numerical Simulation of Leading Edge Receptivity of Stetson's Mach 8 Blunt Cone Stability Experiments," AIAA Paper 2003-1133, 2003. doi:10.2514/6.2003-1133.

[18] Zhong, X., and Ma, Y., "Linear and Nonlinear Boundary-Layer Stability on A Blunt Cone at Mach 8," AIAA Paper 2002-2849, 2002. doi:10.2514/6.2002-2849.

[19] Egorov, I. V., Fedorov, A. V., and Soudakov, V. G., "Direct numerical simulation of disturbances generated by periodic suction-blowing in a hypersonic boundary layer," *Theoretical and Computational Fluid Dynamics*, 2006, pp. 41–54. doi: 10.1007/s00162-005-0001-y.

[20] Poggie, J., Adamovich, I., Bisek, N., and Nishihara, M., "Numerical Simulation of Nanosecond-Pulse Electrical Discharges," *Plasma Sources Science and Technology*, Vol. 22, 2013, 015001.

[21] Poggie, J., Bisek, N., and Gosse, R., "Resolution Effects in Compressible, Turbulent Boundary Layer Simulations," *Computers and Fluids*, Vol. 120, 2015, pp. 57–69. URL `https://doi.org/10.1016/j.compfluid.2015.07.015`.